ELSEVIER

Soil Dynamics and Earthquake Engineering 23 (2003) 549–562

SOIL DYNAMICS AND EARTHQUAKE ENGINEERING

www.elsevier.com/locate/soildyn

Nonlinear soil response as a natural passive isolation mechanism. Paper II. The 1933, Long Beach, California earthquake

M.D. Trifunac*

Department of Civil and Environmental Engineering, KAP 216D Vermont Avenue, University of Southern California, Los Angeles, CA 90089-2531, USA

Abstract

The areas that experienced large strains and differential motions in the soil (indicated by breaks in the water and gas pipe distribution systems) and the areas with severely damaged buildings showed remarkable separation during the March 10, 1933, Long Beach, California earthquake. With analogous results for the 1994 Northridge, California earthquake [Soil Dynam. Earthquake Engng. 17 (1998) 41], the observations summarized in this paper show the fallacy of simplistic and popular interpretations, such as those that hold that in the near field the damage to buildings is caused by 'soft' or 'bad ground' conditions. In fact, significant reduction in the potential damage to buildings may be expected in the areas where the soil experiences 'moderate to large' strains.

Keywords: Nonlinear soil response; Lurching; Breaks in pipe distribution system; Damaged buildings

1. Introduction

Perusal of many papers dealing with the effects that local site conditions have on the distribution of earthquake damage leads to a simple general conclusion: *many published interpretations of damage are imprecise, and often they follow the consensus rather than the trends indicated by the data*. Hauksson and Gross [1], for example, stated that the 'damage was mostly caused by soft, near-surface ground conditions.' The authors did not specify what damage they were referring to, but it is obvious that they meant the damage of buildings during Long Beach Earthquake. Wood [2] stated that "it is obvious, as on previous occasions, that much of the spectacular structural damage was due (1) to bad natural ground or grading-made land, or to deep water-soaked alluvium or sand; and (2) to bad or unsuitably designed construction…" Neumann [3] stated that the "greatest damage occurred in the more thickly settled district from Long Beach to the industrial section just south of Los Angeles proper, where water-soaked alluvium and other unfavorable geological conditions were predominant." Another example of a published opinion, which prefer consensus rather than a careful interpretation of the data, is that of Campbell [4], who stated that "Martel [5] observed that the damage of type III buildings located on recent alluvium was somewhat less than to similar buildings on the more consolidated older alluvium. These findings are in apparent contradiction to general observation made by others for the same earthquake [3]."

The purpose of this paper is to emphasize, again, that in the near field, when the amplitudes of strong-motion become significant (e.g. peak ground velocity $v_{max} > 20$ cm/s) the classical approach to site-specific interpretation of strong-motion amplification based on linear wave theories ceases to be valid [6–8]. Another purpose is to show that (1) the energy absorption of incident seismic waves by nonlinear soil response does lead to a reduction of the destructive power of strong-motion, and (2) the areas where this can occur can be identified and mapped prior to future strong shaking. The subject of this paper and most of its findings are closely related to what Trifunac and Todorovska [7] presented for the Northridge, 1994, California earthquake. Therefore, their paper will be referred to as Paper I, while the present paper, which confirms and extends their findings, will be referred to as Paper II.

2. Long beach earthquake, March 10, 1933

2.1. Distribution of reported Mercalli intensities

Intensities as high as IX on the Mercalli scale were reported in the cities of Long Beach and Compton. Intensity

* Tel.: +1-213-740-0570; fax: +1-213-744-1426.
E-mail address: trifunac@usc.edu (M.D. Trifunac).

0267-7261/03/$ - see front matter © 2003 Elsevier Ltd. All rights reserved.
doi:10.1016/S0267-7261(03)00071-X

VIII was reported at 17 sites, VII at 26 sites, VI at 29 sites, V at 26 sites, IV at 80 sites and III and lower at 70 sties. Except for a rough map published in US Earthquakes in 1933 (page 10 in Neumann [3]) and a single intensity 'contour' for intensity VIII in Ref. [9], it seems that no detailed isoseismal map was published for Long Beach, 1933, earthquake.

Fig. 1 shows the current author's interpretation of the reported intensities in Neumann [3], for the range of intensities between III and IX. For comparison, this figure shows also the zone of aftershocks that followed the March 10 earthquake (shown by an oval hatched zone) and two asperities hypothesized on the basis of teleseismic recordings of the main event [1]. Our isosesmals for intensities VII and VIII show two lobes, one directed toward north–northeast, emanating from the epicentral region (near the southeastern end of the large asperity), and the other directed toward north–northwest, in the direction of the cities of Long Beach and Compton.

It can be seen from Fig. 1 that the intensity of shaking attenuated rapidly in the direction perpendicular to the long axis of the aftershock zone (toward north and northeast). Overall, isoseismals were elongated toward northwest, implying fault rupture propagating toward the northwest. Fig. 1 also shows the locations of damaged chimneys most remote from epicenter [10], and intensity VI, extending 70 miles (112 km) to the north-west, up to Ventura and only 20 to 25 miles (40 km) southeast, up to San Juan Capistrano.

2.2. Newport-Inglewood fault zone

The Newport-Inglewood structure is a deep-seated, northwesterly trending zone of folds and faults, accompanied by dome-shaped hills and low mesas [11, 12]; Figs. 2–4). It extends about 40 miles (64 km), from Newport Mesa in Orange County, up to and through Baldwin Hills, near Culver City in Los Angeles County. The hills (north to south), are Baldwin, Rosecrans, Dominguez, Signal, Reservoir, Landing, Bolsa Chica Mesa, Huntington Mesa, and Newport Mesa (Figs. 3 and 4). They are the surface expressions of geologic deformations since the mid-Tertiary (20–30 million years ago).

The Newport-Inglewood fault is a boundary between metamorphic basement to the west and metamorphosed sediments and plutonic and volcanic rocks to the east. It belongs to the faults which form the San Andreas Fault system, with overall right lateral slip motion between the North American and Pacific plates. Since the mid-Miocene (12–26 million years ago), the cumulative right lateral offset along the Newport-Inglewood fault has been 3 km [13]. Within the area of this study, along the low-lying Dominguez, Signal, Reservoir, and Landing hills, and the Bolsa Chica Mesa (Figs. 3 and 4), en-echelon fault segments, and numerous oil fields are located adjacent to and along the Newport-Inglewood fault (Fig. 2). The fault has a steep, dipping angle towards the northeast, near Long Beach, and becomes almost vertical near Seal Beach. Near Sunset Beach, it dips steeply to the southwest (see Fig. 8 in Ref. [1].

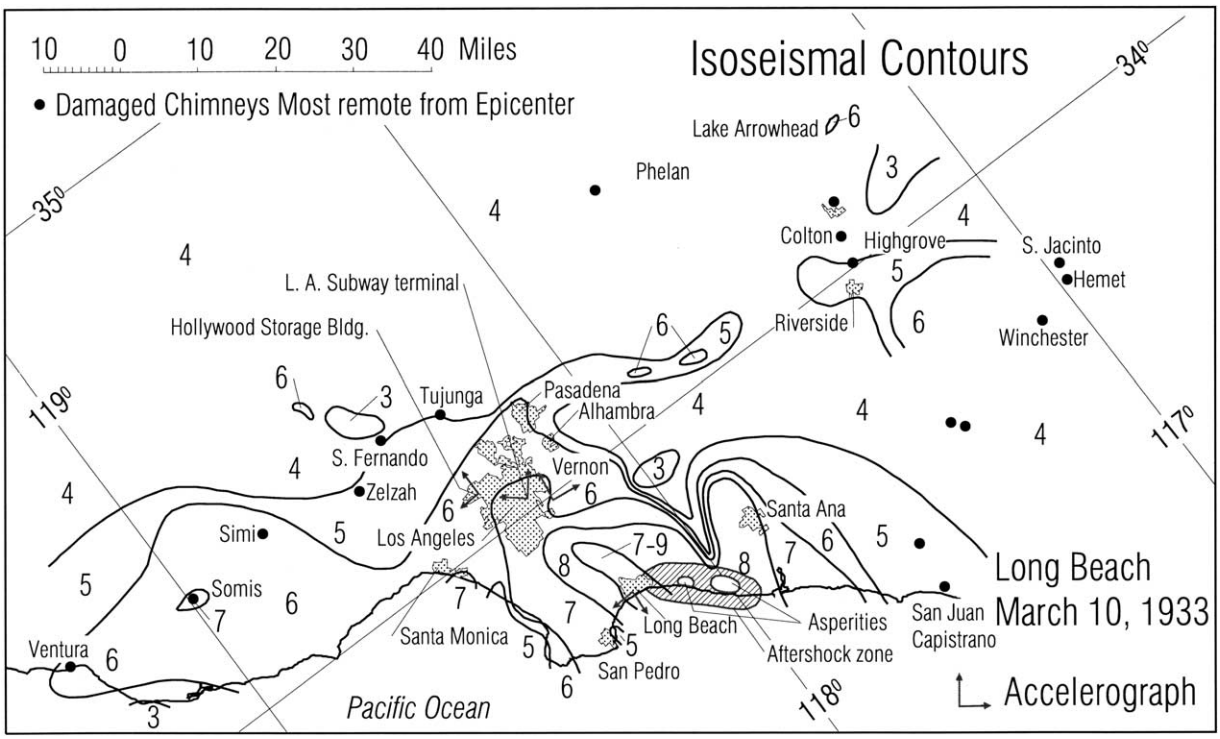

Fig. 1. Distribution of Mercalli intensities during March 10, 1933, Long Beach, California earthquake.

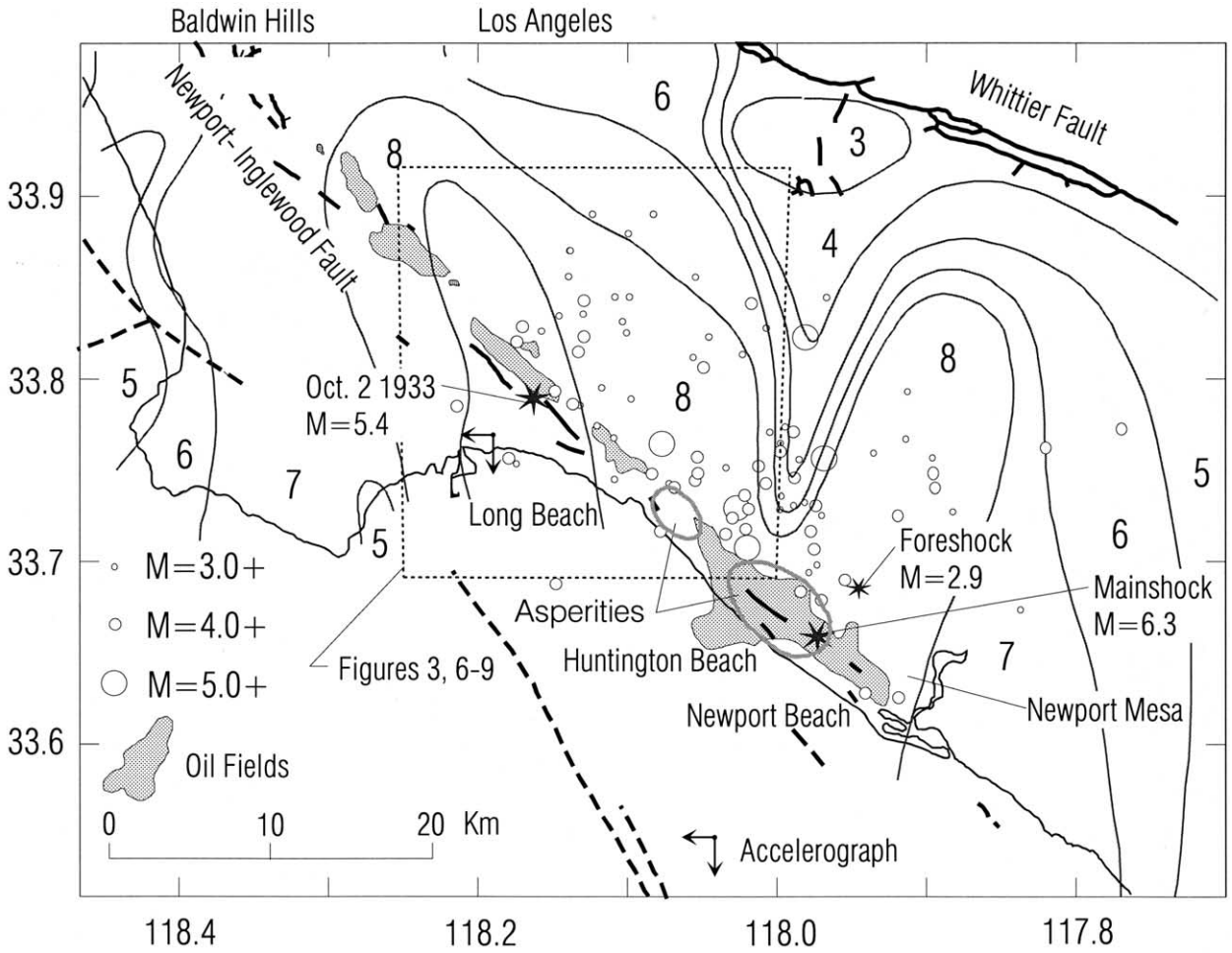

Fig. 2. Aftershocks of Long Beach earthquake (redrawn from Ref. [1] along Newport-Inglewood fault zone.

Production of petroleum started in 1920, and within 4 years it spread to Long Beach (1921), Dominguez (1923), Rosecrans (1924), Seal Beach (1924) and Inglewood (1924). Subsidence along the portions of Newport-Inglewood fault zone was caused by withdrawal of fluids and by tectonic deformations. This creates problems with construction and operation of drainage channels, sewers, and pipelines. This subsidence ranges from 2 ft in Long Beach (between 1928 and 1965) to 5.1 ft in Huntington Beach (between 1920 and 1965), and to 5.7 ft in the Inglewood oil field (between 1911 and 1963).

Following the March 10, 1933 earthquake, no surface expression of the fault motion was seen on the surface, but numerous cracks opened in alluvium within the heavily shaken area [14] and particularly in *the Alamitos Bay–Seal Beach area and in unconsolidated sands of the Los Angeles River flood plain in Compton. Water was ejected from sandy and muddy alluvium and sand boils or mud 'volcanoes' formed in the Alamitos–Seal Beach area near the Newport-Inglewood structural area, near the mouth of the Santa Ana River and at Cabrillo Beach (San Pedro)…* Those features, are *most logically explained as being caused by 'lurching,' that is, inelastic response of unconsolidated water-saturated materials to ground motion during earthquake* [11].

2.3. Seismological studies

The Long Beach earthquake occurred on March 10, 1933, at 5:54 p.m., PST. The original epicenter, calculated by hand, was at 33°34.5′N and 117°59′W, about 5.6 km (3.5 miles) southwest of Newport Beach [2]. The main shock was preceded by a foreshock ($M_L = 2.9$) on March 9, less than 4 km to the north of the main event (Fig. 2). The Long Beach earthquake then followed at 0154 UT, on March 11, 1933, at 33°39.54′N latitude and 117°58.30′W longitude, at a depth of 13 km. It had magnitude $M_L = 6.3$. Its focal mechanism can be described by dip direction of 45°, dip of 80° and rake of −170°. Seismic moment was estimated at 5×10^{25} dyne cm. The rupture was unilateral, propagated from the hypocenter towards the northwest, along the Newport-Inglewood fault, causing right-lateral strike slip

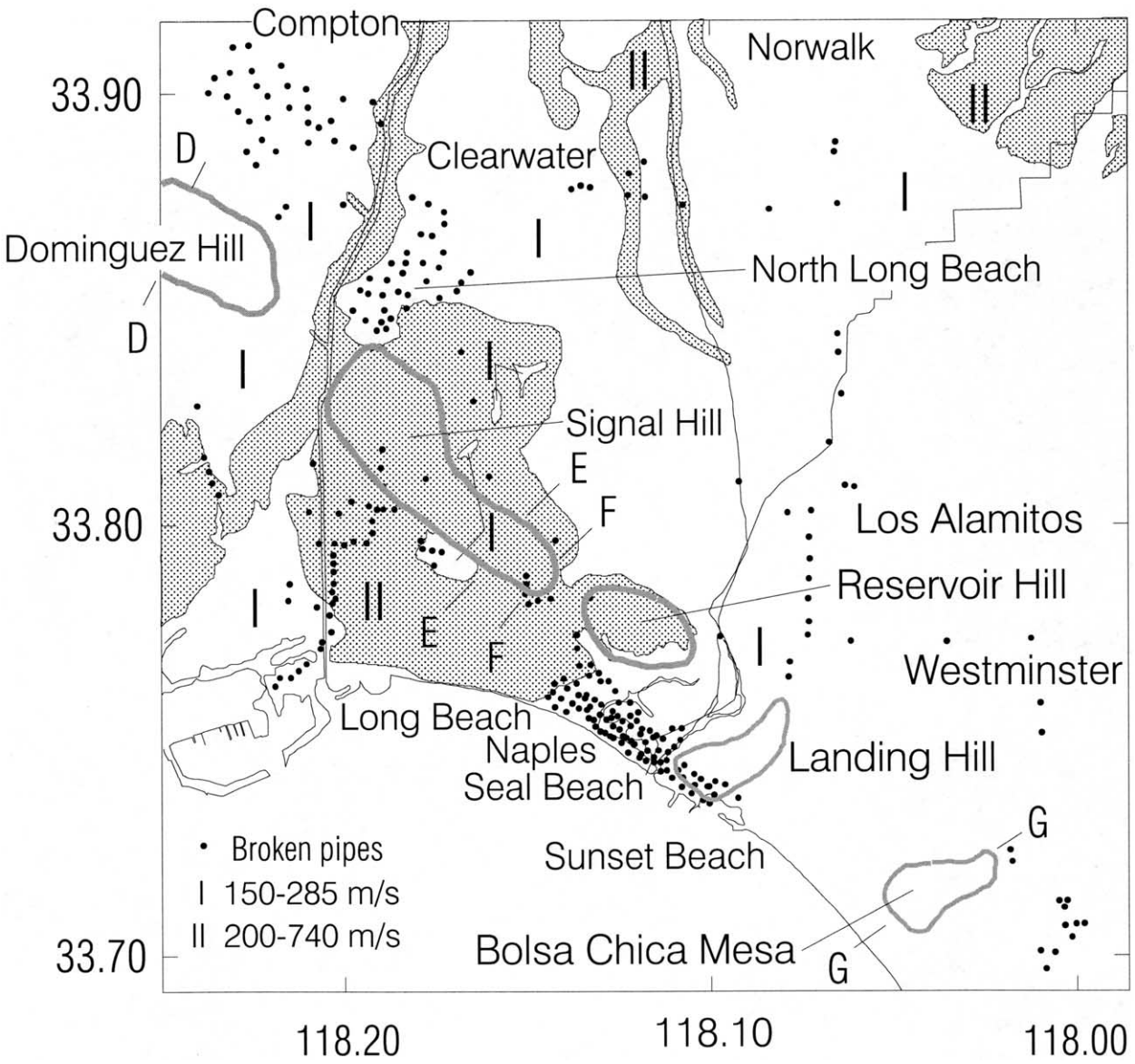

Fig. 3. Distribution of pipes broken during March 10, 1933 Long Beach earthquake (redrawn from Ref. [25], outline of Hills (Dominguez, Signal, Reservoir, Landing, and Bolsa Chica Mesa), and distribution of shear-wave velocity in the soil (I, 150–285 m/s; II, 200–740 m/s), along Newport-Inglewood fault zone.

motion, with a minor normal component [1]. The aftershock zone extended from Newport Beach to Long Beach. The distribution of aftershocks showed two clusters, one 7–9 km north of focus, and the other 13–16 km northwest. Hauksson and Gross [1] interpreted this distribution of aftershocks to be caused by the breaking of two asperities (shown by two ovals in Figs. 1 and 2) during the main event, one 6–8 km long between hypocenter and the first cluster, and the other 3–4 km long between the first and second cluster of aftershocks. Their interpretation is consistent with our isoseismal contours for the main event.

Analysis of teleseismic data indicates that the duration of the main event was about 5 s [1], which is in agreement with reported duration of strong shaking (5–10 s in Pasadena, Ref. [2].

2.4. Strong-motion data

Strong ground motion during the main event was recorded by three accelerograph stations at (1) the Long Beach Public Utilities Building, (2) the Vernon CMD Building, and (3) the Los Angeles Subway Terminal (Figs. 1 and 2). Instrument and baseline-corrected strong-motion data from these sites are presented in [15,16]. Table 1 summarizes peak accelerations, velocities and displacements of band-pass-filtered data [17]. It can be seen that the largest peaks were recorded at Long Beach, all on the vertical component of strong-motion (279 cm/s^2, 29.5 cm/s, and 26.4 cm for acceleration, velocity, and displacement, respectively). The significance of this strong-motion data is that it represents the first strong-motion recording in

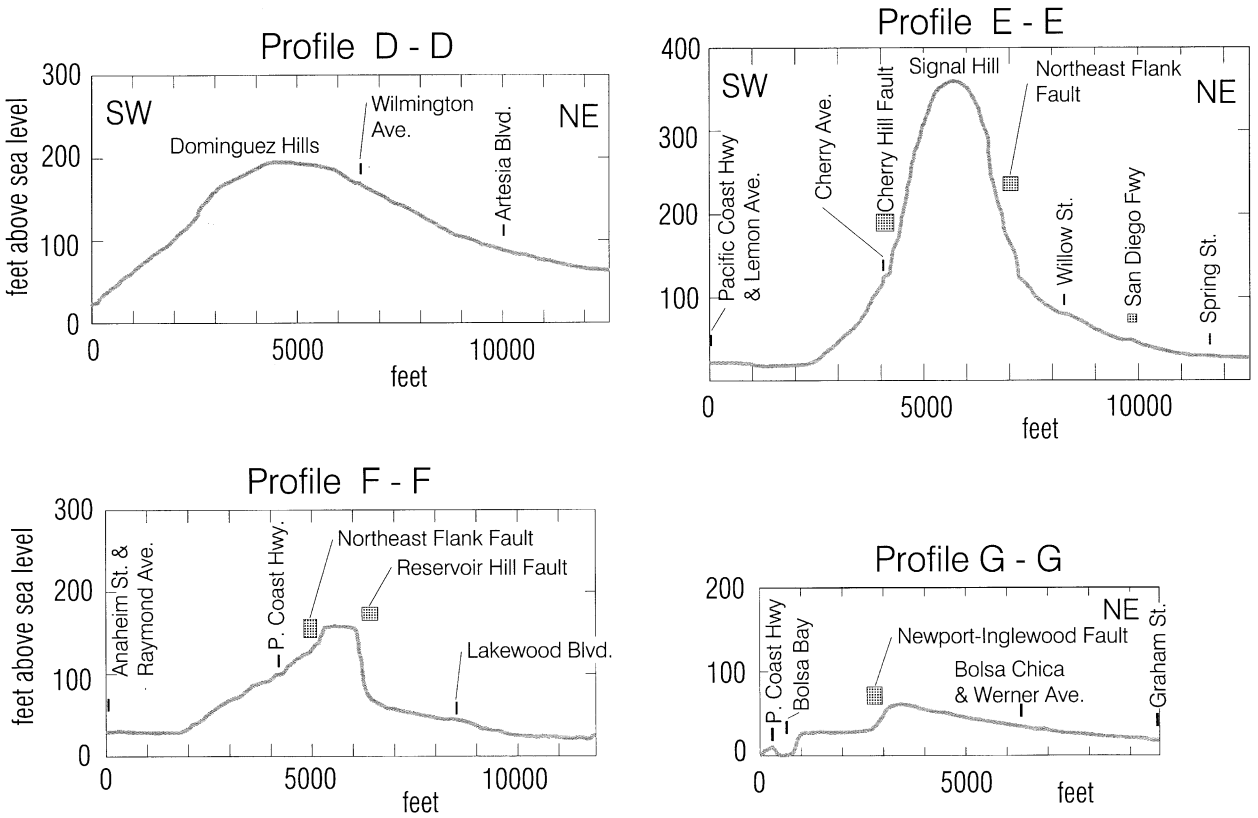

Fig. 4. Cross-sections of topography across Dominguez, Hill (D–D), Signal Hill (E–E and F–F), and Bolsa Chica Mesa (G–G) (Fig. 3).

the history of earthquake engineering [18]. The number of recording stations and their position relative to the causative fault was not adequate to allow inverse source mechanism studies of this event [19], but the closest station, at the Long Beach Public Utilities Building, can be used qualitatively to infer the most elementary spectral features of the source.

Fig. 5 shows Fourier amplitude spectra of two horizontal (south and west) and one vertical component of strong-motion displacement recorded at Long Beach. To account for high frequency attenuation, the spectral amplitudes were multiplied, before plotting by $\exp(\omega\Delta/2Q\beta)$. It has been assumed that hypocentral distance, Δ, is about 22 km, $Q \approx 350$, and $\beta \approx 3$ km/s. This correction is significant only for high-frequency spectral amplitudes higher than about 5 Hz (32 rad/s).

As can be seen from Fig. 2 the strong-motion instrument at Long Beach Public Utilities Building was about 25 km northwest of the epicenter and less than 5 km from the northern end of the fault rupture, as indicated by the distribution of aftershocks (Figs. 1 and 2). It can therefore be assumed that it recorded mainly near field waves, which were focused toward northwest because of the propagation of fault slip in that direction [1,20].

In the near field, the Fourier amplitude spectrum of strong-motion displacement can be approximated by

$$|F(\omega)| = \frac{\sigma\beta}{\mu} \frac{1}{\omega(\omega^2 + \tau^{-2})^{1/2}}, \tag{1}$$

where σ is the stress drop; β, the velocity of shear waves; μ, the rigidity of rocks in the source region; τ is proportional to the duration of faulting [21,22], and

$$\tau \sim \frac{L}{v} + \frac{W}{2\beta}, \tag{2}$$

where L is source length; W, the source width; v is the velocity with which the dislocation is spreading during the faulting process. $|F(\omega)|$ described by Eq. (1) fits nicely the observed spectra of strong-motion displacement at Long Beach if one assumes $\sigma \sim 90$ bars, $\beta \sim 3$ km/s, $\mu = 3 \times 10^{11}$ dyne/cm^2, and $\tau > 1$ (Fig. 5). For unilateral faulting, this implies that $L > 3$ km.

In the near field, the peak particle velocity, $v_{\max}$, can be approximated by Trifunac [21]

$$v_{\max} \sim \frac{\sigma\beta}{\mu}. \tag{3}$$

Assuming that the earthquake started with failure of the asperity near the epicenter, the peak velocity equal to 30 cm/s recorded in Long Beach (Table 1), resulted from attenuation over the distance of about 22 km, of $v_{\max} \sim 87$ cm/s in the source region. With this, Eq. (3) gives $\sigma \sim 87$ bars, which is in agreement with the above estimate of 90 bars, using Eq. (1).

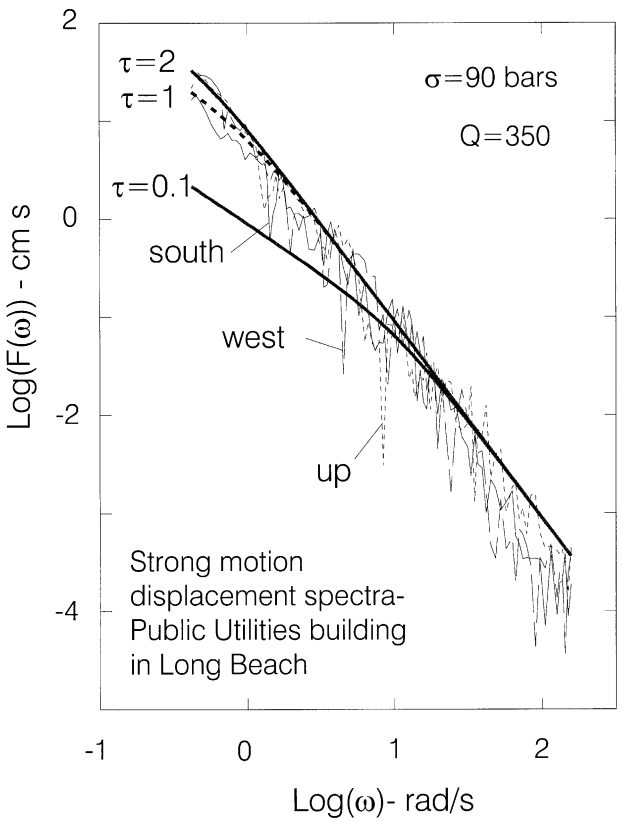

Fig. 5. Near field Fourier amplitude spectra of strong-motion displacement recorded at Long Beach Public Utilities Building (Figs. 1 and 2), corrected for inelastic attenuation (light continuous and dashed lines), compared with theoretical near field spectrum of displacements for stress drop $\sigma = 90$ bars and source 'durations' $\tau = 0.1$, 1 and 2 s.

3. Earthquake damage

The Long Beach earthquake was not a major earthquake, but because of its location in a settled region with poorly constructed buildings, it was one of the most destructive earthquakes in the US history. The damage was estimated at 41 million dollars, and the area affected was 75,000 sq mi (192,000 km^2) (Neumann [3]). Many hundreds of people were injured, and about 120 died. It was reported that up to 19 fires may have resulted from strong shaking (two in Los Angeles), seven of which were attributed to damaged gas pipes and devices [23,24].

3.1. Building damage

Martel and his students investigated the earthquake damage of the buildings designated as class 'C', in older building codes and as type III in the uniform building code. These buildings were of ordinary masonry construction with exterior masonry bearing walls and with interior load-bearing construction of wood, steel, or masonry. At the time of the earthquake, practically all type III buildings were of brick construction [10]. The method employed to quantify damage was to *determine the relation in percent between the total assessed value of type III buildings only and the total adjusted reductions in assessed value for each block. These percentages varied from 3 to 90, and were arranged in five groups:* (1) 0–9%, (2) 10–17%, (3) 18–22%; (4) 23–30%, and (5) 30–100%. Each group was designated by different cross hatching on the map (see Fig. 109 in Ref. [10]. Martel's data is reproduced in Fig. 6, where various symbols are plotted in the center of damaged blocks, corresponding to the above five groups, as follows: (1) 0–9% damage is shown by a light open circle, (2) 10–17% damage is shown by a light triangle, (3) 18–22% damage is shown by a light square; (4) 23–30% damage is shown by heavy triangle, and (5) >30% damage is shown by a heavy square.

Martel [10] next correlated the building damage with soil conditions and *observed that the damage to type III buildings located on the softer, more recently deposited alluvium with ground water at from 2 to 10 ft from the surface is somewhat less than to similar buildings on the slightly older, firmer alluvium, with groundwater not so*

Table 1
Peak strong-motion amplitudes recorded during March 10, 1933, Long Beach, California earthquake

	Component	Peak acceleration (cm/s)	Peak velocity (cm/s)	Peak displacement (cm)	Source
Long Beach Public Utilities Building, 33.77N, 118.19W	South	192.7	−29.3	22.7	EERL 75-52 [16]
	West	−156.0	15.8	11.9	
	UP	279.0	−29.5	−26.4	
Vernon CMD Building, 33.99N, 118.20W	N08E	130.6	28.7	−15.5	EERL 72-50 (Trifunac [15])
	S82E	−151.5	17.0	−17.5	
	UP	149.5	12.0	7.4	
Los Angeles Subway Terminal sub-basement, 34.03N, 118.25W	N39E	62.3	−17.3	−8.2	EERL 75-52 [16]
	N51W	95.6	−23.7	−16.3	
	UP	63.6	9.1	−5.7	

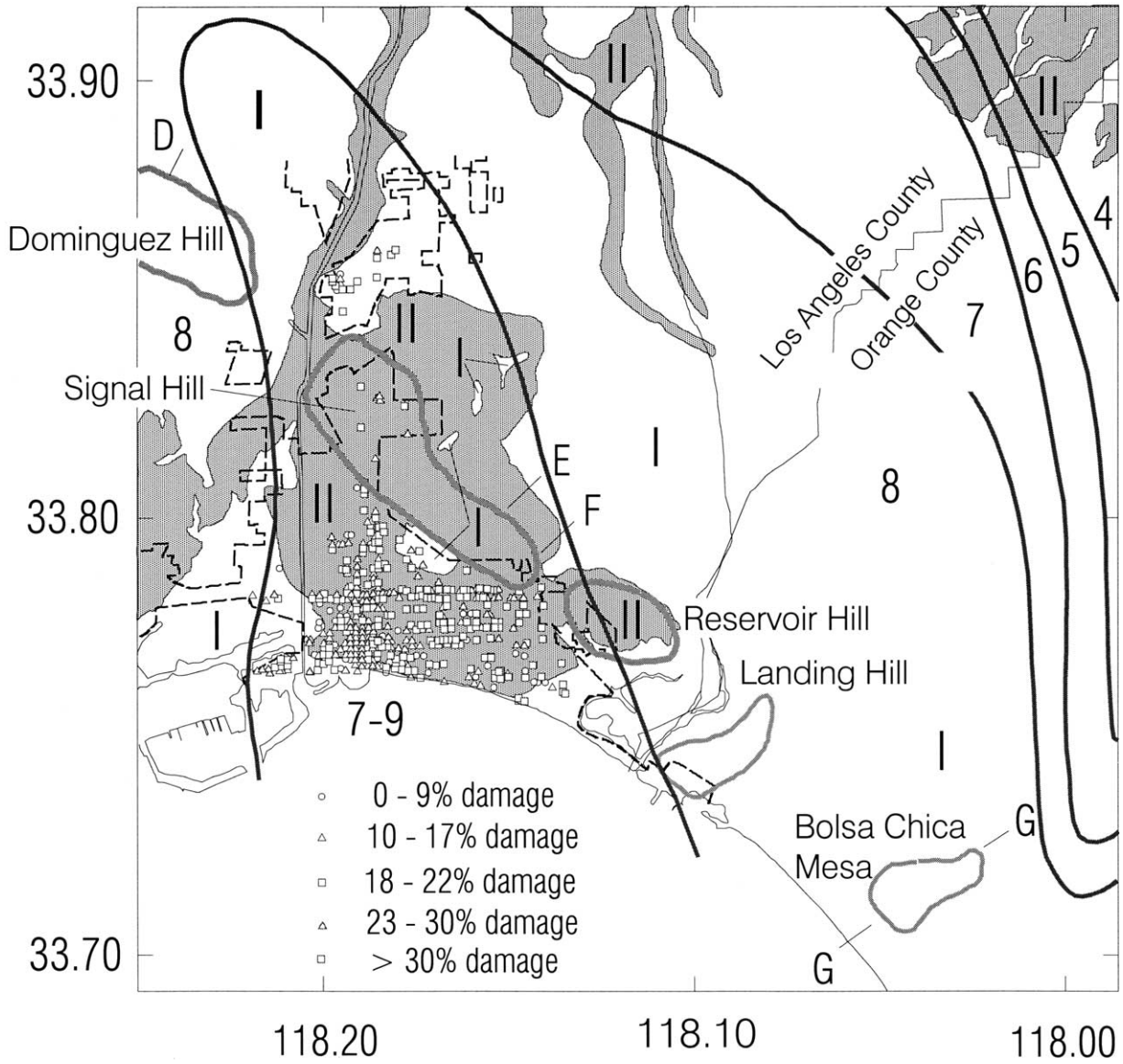

Fig. 6. Distribution of blocks with damaged buildings (open circles, triangles, and squares; redrawn from Ref. [10], relative to reported site intensities (IV–IX), and distribution of shear-wave velocities near surface (I, 150–285 m/s; II, 200–740 m/s).

close to the surface. Areas of lesser damage are found both at the west end of the city along the old riverbed and in the southeast section bordering on Alamitos Bay. Damage along the beach, below the bluff, was also less than on higher ground.

3.2. Damage of pipelines

Fig. 3 shows the breaks in water and gas lines caused the by Long Beach earthquake [25]. The areas with the highest concentrations of breaks were in Seal Beach, in north Long Beach, and in Compton.

The following citation from Ref. [25] describes the areas of concentrated pipe breaks, and the relationship of these breaks to the local soil conditions: *By plotting the main line breaks on a map, as shown in Fig. 3, it becomes fairly evident that the nature of the soil in which the pipes were laid had an important bearing upon their failure. For example, the area of greatest breakage was at the mouth of the San Gabriel River in the Alamitos Bay District, particularly in the regions known as Belmont Shores, Naples, and North Seal Beach. This entire area, before being settled, was one great swampy lowland, wholly or partially inundated at high tide. The water table is still within a few feet of the surface, and it is interesting to note that it was in this vicinity that there were formed small sand craters which are often found in earthquakes of greater violence, sometimes of great size, in locations where the soil is soft or sandy and the water is fairly close to the surface. In the Charleston earthquake of 1886, sand craters were*

formed which were as much as 10 feet across and threw out tremendous amounts of water and sand. It was in this Alamitos Bay region of water-soaked silt, loam, and sand that there occurred upward of one third of the total number of pipeline failures which were recorded in the Long Beach earthquake of March 10, 1933.

The area of next greatest breakage was in the North Long Beach, Compton, and Clearwater vicinity. It seems that during the past 200 years the Los Angeles River has many times changed its course in this neighborhood, so that this entire area has taken on the characteristics of a dry streambed. Then, too, the Rio Hondo River and Compton Creek empty into the Los Angeles River at this point, and old maps show that there were formerly several small lakes, principally Bouton Lake, as well as a series of artesian springs and wells at this location. Although pipeline failures were exceptionally numerous in this territory, they were not so concentrated as in the area first described.

In addition to these two principal areas, it was noticeable that breaks were numerous along the banks of the creeks, rivers, and flood control channels all along the coastal plain.

3.3. Breaks in underground system

In the system of 410 miles of pipe lines, 119 major breaks were found before the gas service could be resumed [26]. *Of 91 breaks in the high-pressure system, over 50 were in the filled-in land area, and in every case they were due to failure of the welded joint. Forty-six breaks were discovered in the large diameter (18- and 29-in.) main in the Harbor district… At one point, the earth movement…was so great that there remained a gap of 8 inches to fill in…before the pipe line could be restored to service.*

There were more than 500 breaks of water, gas, and oil lines [25]. In the Long Beach gas distribution system there were 119 main breaks. Of those, 91 were in the high-pressure mains [26].

3.4. Breaks in service lines and risers and at meters

During the earthquake 2200 buildings were jolted off foundations or demolished. About *1650 services had broken risers or breaks at the connection to meter or regulator. Approximately 1000 services were sheared off at the connection at the main. Over 90 percent of the total number that pulled apart or sheared off was located in loose filled-in ground in the Naples district. Out of a total of 3000 consumers in the district, approximately 900 services were broken either at the riser, at the main, or both. The district—about two miles long by one mile wide—lies in an area entirely built up from tide lands, and the soil is composed entirely of sand, with a water table at high tide only 40 in. below the surface. It was in this district, too where the result of the earth movement could readily be seen from broken pavement and displaced walks* [26].

4. Results and interpretation

During the main shock, the rupture started just north of Newport Beach (Fig. 2) and then propagated toward the northwest, along the Newport-Inglewood fault [20]. Teleseismic source studies, and distribution of reported intensities (Fig. 1) are consistent with a source duration of 5–6 s [2] and source representation in terms of two major asperities, one near the focus and the other 5–10 km northwest along the fault (Fig. 2). This source resulted in focusing of strong-motion energy toward northwest, in the direction of Long Beach and Compton, causing damage and destruction to structures and causing large, nonlinear responses in 'soft' soils (Figs. 3 and 6–9). The strong-motion accelerograph in Long Beach (Fig. 2) recorded the largest peak acceleration, velocity, and displacement in the vertical direction (Table 1: 279 cm/s^2, 29.5 cm/s and 26.4 cm, respectively). Spectral amplitudes of this record are consistent with stress drop on the fault of about 90 bars. This amplitude of stress is of the same order as the stress drop during the San Fernando, California, earthquake of 1971 [21], and the Northridge earthquake of 1994 [27], suggesting that the high-frequency spectral amplitudes of strong-motion in Long Beach were as high as the other 'largest' near-field spectral amplitudes recorded so far [28,29].

Damage to structures begins to take place for strong-motion with peak velocities larger than 10–20 cm/s [30], and the water pipes (depth of burial 2–4.5 ft; 0.6–1.4 m) begin to break for $v_{max} \geq 15$ cm/s at sites with average shear wave velocity near the surface of $\bar{\beta} \leq 300$ m/s—that is, for surface strains larger than $\sim 10^{-3}$ [7,31]. The structures in Long Beach were designed before the Field act of 1934, and thus their damage during the earthquake cannot be compared directly with observations of damage during subsequent earthquakes in the Los Angeles metropolitan area. Yet, there should be no doubt that the high-frequency amplitudes of strong shaking in Long Beach were 'large' and comparable to the strongest levels of shaking during the San Fernando and Northridge earthquakes, thus producing significant damage to structures [10], and water, gas and oil pipelines [25].

The remarkable feature of the spatial relationship of the areas with damaged buildings to the areas with broken pipes is that they essentially did not overlap. A few overlaps did occur, such as near the intersection of Pacific Coast Highway and Los Alamitos Avenue in Long Beach and near the intersection of South Street and Atlantic Avenue in North Long Beach (Figs. 3 and 6–9), but in general these areas were the exception.

The majority of the damaged buildings were located in the areas of relatively higher average shear wave velocity in the soil (II: 200–740 m/s, see Fig. 3), with low (L) to very low (VL) liquefaction susceptibility. Pipe breaks generally occurred in the areas with relatively low average shear wave velocity near the surface (I: 150–285 m/s, see Fig. 3), with

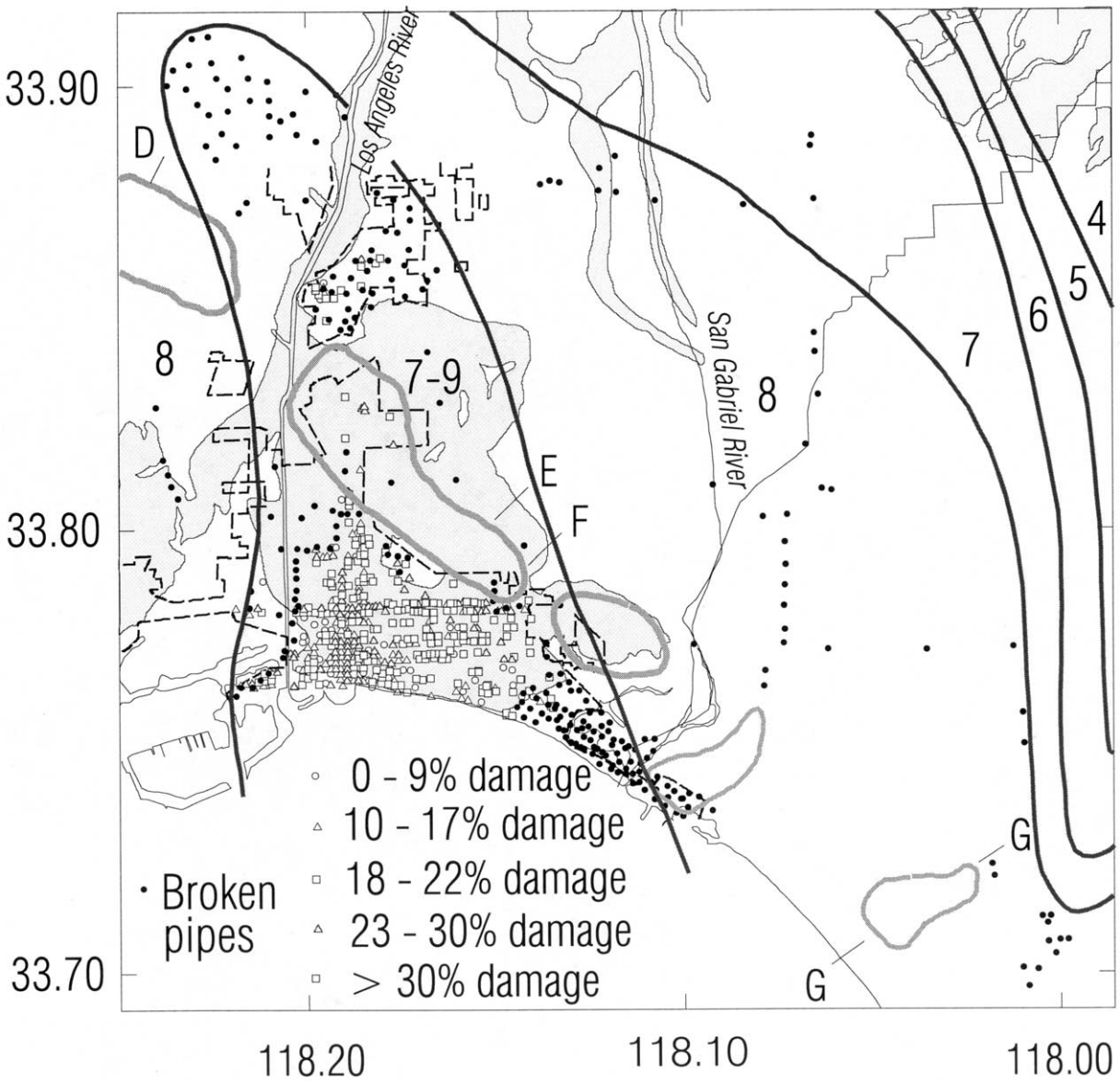

Fig. 7. Comparison of the areal distributions of broken pipes (Fig. 3) and blocks with damaged buildings (Fig. 6).

very high (VH) and high (H) liquefaction susceptibility. These observations apply only within the boundaries of the Los Angeles County (Fig. 6), roughly west of the San Gabriel River. The reason for this is that at the time of this writing the maps with shear wave velocities (Fig. 3) and liquefaction susceptibility of the sites (Figs. 8 and 9), were available in published literature only for Los Angeles County [32]. For completeness of this presentation, we have plotted the locations of all pipe breaks in Orange County as well (Figs. 3 and 6–9).

There appear to exist no published results on the damage to buildings in Orange County during the 1933 Long Beach earthquake with the detail and quantification of damage such as presented by Martel [10] for the Long Beach area. Likewise, there are no comparable studies published on building damage in Compton, where the damage was severe and perhaps even greater than in Long Beach [2]. The areas covered by the Martel [10] study of damaged buildings are outlined by dashed lines in Figs. 6–9, and our observations apply only within those boundaries. Nevertheless, the distribution of pipe breaks in Compton is consistent with such areas in Long Beach—that is, the average shear wave velocities in the soil were 150–285 m/s (Zone I)—and in the 1930s Compton appears to have been in the area of very high (VH) liquefaction susceptibility.

We observed similar areal separation of the zones with damaged buildings and the zones with broken pipes following Northridge earthquake of 1994 [7]. The fact that this separation occurred so clearly during the Long Beach earthquake of 1933 reinforces our expectation that

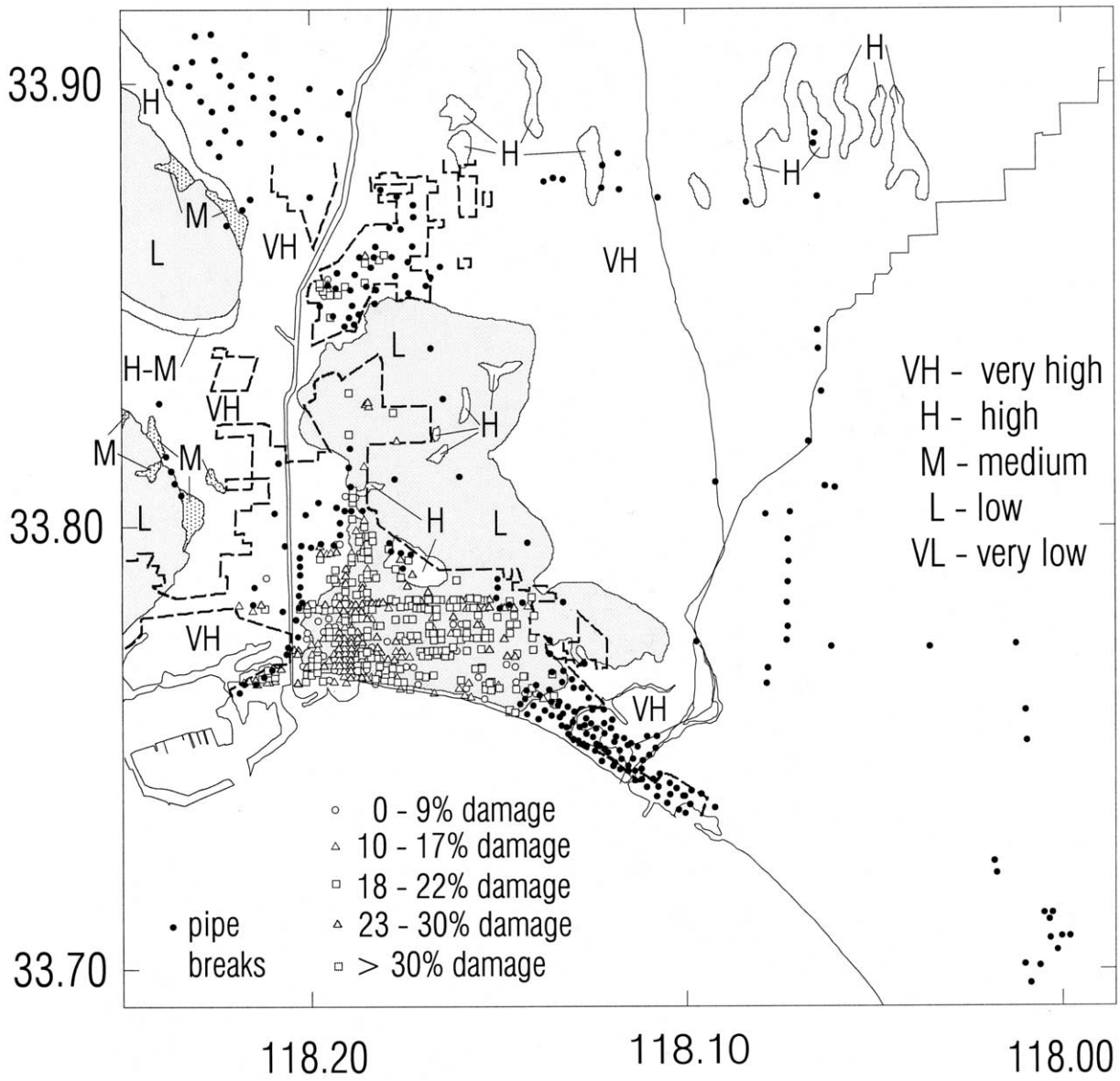

Fig. 8. Distribution of broken pipes and blocks with damaged buildings relative to the areas of liquefaction susceptibility, very low (VL) to very high (VH), for the period preceding 1940s.

the underlying physical mechanism may be general and widespread in the urban areas of metropolitan Los Angeles.

5. Discussion and conclusions

The foregoing shows that the near surface deposits play a significant role in modifying the effects of strong-motion shaking in the near field. Also, the areas likely first to experience nonlinear deformations in the soil during future strong shaking can be identified and mapped in advance. The best and most rational guidelines on how to characterize and identify the relevant and critical site conditions, variations in near-surface shear velocity, and liquefaction susceptibility come from observations of the effects of past earthquakes, as shown in the above examples for the 1933 Long Beach event. The data on broken pipelines and damaged buildings exist for many other past earthquakes as well. The challenge for future research is to reconstruct this data from old papers and reports and to interpret the spatial relationships in terms of the local geologic and soil site conditions.

5.1. Site conditions

The surface deposits within the area shown in Figs. 3 and 6–9 are Quaternary. The Pleistocene strata have thickness between 200 and 400 m, are mainly of marine origin (Poland [33]), and consist of slightly to moderately

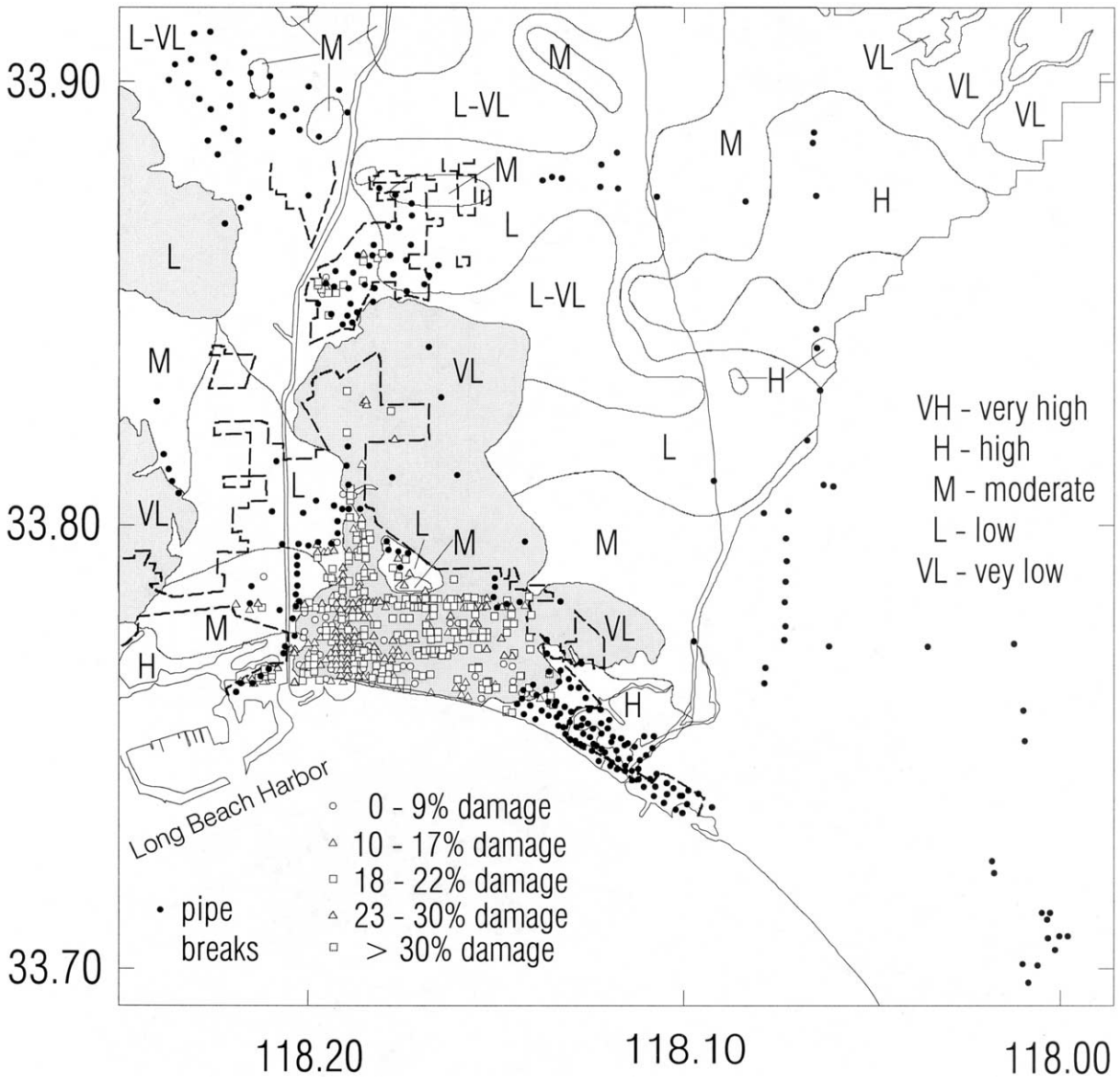

Fig. 9. Distribution of broken pipes and blocks with damaged buildings relative to the areas of liquefaction susceptibility, very low (VL), to very high (VH), for the period after 1940s.

consolidated beds of silty sand, clayey sand, and sandy silt. Up to 50 m of Holocene sediment occurs in the valleys eroded by streams. The upper parts of Holocene deposits usually are fine grained and consist mainly of unconsolidated to partly consolidated deposits of sand, silt, and some clay, mixed with estuarine and marsh deposits near the coastline. Lense deposits composed of medium to coarse sand and gravel occur occasionally in upper Holocene but predominate at depths of 5–12 m in Holocene, which is designated as the Gaspur aguifer zone [33–35]. Subjacent Tertiary sediments are composed of shale, siltstone, chert, and limestone. At a depth of 2100 m in the southwest corner of Figs. 3 and 6–9, the Tertiary section overlies the northwest-trending axis of Wilmington anticline, so that the depth to the basement ranges from 2100 m near Terminal Island to 6100 m near Compton [36]. West of the Newport-Inglewood fault zone, the Tertiary layers lie over the Catalina shist.

5.1.1. Variations in near-surface shear-wave velocity

The classical approach to interpretation of areal differences in damage caused by strong shaking begins with the study of the variations in near-surface geology [37–40] and aims to interpret observations in terms of the variations in shear-wave velocity and in the associated impedance. An approach for mapping areal variation in wave velocity can begin with mapping Quaternary sedimentary deposits, grouped according to their age and grain size. Next,

Table 2
Comparison of relative bulk density, penetration resistance, shear-wave velocity, and calculated impedance values of surficial geologic units (from Ref. [32])

Geologic unit	Bulk density[a] (g/cm^3)	Average penetration[b] (blows/ft)	Shear-wave velocity[c] (m/s)	Shear-wave velocity group	Shear-wave impedance[d] ($V_S\rho$)
Holocene (less than 10,000 years old)					
Qyf (fine-grained Holocene alluvium)	1.6 ± 0.2	14 ± 8	150–270 (200)	I	210–490 (320)
Qym (medium-grained Holocene alluvium)	1.6 ± 0.2	14 ± 8	195–285 (230)	I	270–510 (370)
Qyc (coarse-grained Holocene alluvium)	1.6 ± 0.2	–	290–355 (320)	II	410–640 (510)
Qyvc (very coarse grained Holocene alluvium)	1.6 ± 0.2	–	350–375 (365)	II	490–675 (580)
Pleistocene (10,000–1,700,000 years old)					
Qof (fine-grained Pleistocene alluvium)	1.9 ± 0.3	34 ± 18	200–360 (305)	II	320–790 (580)
Qom (medium-grained Pleistocene alluvium)	1.9 ± 0.3	34 ± 18	270–740 (430)	II	430–1630 (820)

(–) no data available.
[a] Bulk densities (ρ) for Quaternary deposits from Ref. [46] and Los Angeles County Flood Control District (unpublished data, 1950–1980).
[b] From CALTRANS freeway borings; 5- to 10 ft subsurface, 140 lb hammer, 30 in. drop. Penetrometer tests not reliable in gravelly and bouldery deposits. Refusal indicates failure to advance the penetrometer through the Earth materials.
[c] Holocene and Pleistocent values from Ref. [47]. Mean values in parentheses.
[d] Mean values in parentheses.

the sediment age and grain size can be correlated with shear-wave velocity [32,41]. Table 2 shows the results of such correlations for the materials found in the areas of heavy building damage and breaks in water and gas pipes following the 1933 Long Beach earthquake, while Fig. 3 shows the distribution of 'low' (I) and 'intermediate' (II) velocity zones. It is seen that the damage to buildings is essentially confined to the 'stiffer' and 'stronger' site materials, while breaks in the pipes occur in 'soft material' with 'low' shear-wave velocity (I).

The fallacy of many published interpretations of observed damage lies in their attempt to relate damage to the expected linear amplification of seismic waves entering 'soft' surface deposits. While this approach is certainly correct for 'small' amplitudes of motion ('small' strains in the soil), it ceases to be a valid representation for large amplitudes of strong-motion, when surface deposits undergo nonlinear response. This was demonstrated, for example, using the data gathered after the 1994 Northridge earthquake (Trifunac and Todorovska [8]), and is consistent with the data on the 1933 Long Beach, earthquake presented here.

5.1.2. Liquefaction susceptibility

Four types of ground failure can follow liquefaction: lateral spreading, ground oscillations, flow failure, and loss of bearing strength. *Lateral spreads* involve displacements of surface blocks of sediment facilitated by liquefaction in a subsurface layer. This type of failure may occur on slopes up to 3° and is particularly destructive to pipelines, bridge, piers and other long and shallow structures situated in flood plain areas adjacent to rivers. *Ground oscillations* occur when the slopes are too small to result in lateral spreads, following liquefaction at depth. The overlying surface blocks break one from another and then oscillate on liquefied substrate. *Flow failures* are a more catastrophic form of material transport and usually occur on slopes greater than 3°. The flow consists of liquefied soil and blocks of intact material riding on and with liquefied substrate, on land or under the sea (e.g. at Seward and Valdez during the 1964 Alaska earthquake). *Loss of bearing strength* can occur when the soil liquefies under a structure. The buildings can settle, tip, or float upward, if the structure is buoyant.

Surficial geologic map (considering age and type of sedimentary deposits) and maps showing depth to ground water can be superimposed to derive liquefaction susceptibility maps. Depending upon climate conditions and water use, liquefaction susceptibility can increase during wet cycles and decrease during dry cycles.

To asses liquefaction susceptibility, Timsley et al. [42] subdivided the late Quaternary deposits in the Los Angeles region into three stratigraphic units according to their relative age: (1) latest Holocene deposits, less than 1000 years old, and typically less than 4 m thick; (2) earlier Holocene deposits, between 1000 and 10,000 years old; and (3) undifferentiated later and middle Pleistocene marine and nonmarine deposits, younger than 0.5 million years.

Fig. 8, reproduced from Ref. [42] shows a 'high water level' liquefaction susceptibility map, assuming that the depth to ground water is approximately as described by Mendenhall [43,44]. Flood plain areas with the latest Holocene deposits of cohesionless, granular sediments are assigned very high (VH) susceptibility. As the sediment becomes older or as the depth to ground water increases, the liquefaction susceptibility is reduced. Tinsely et al. [42] indicated that the ground water data up to the mid-1940s approximate the high ground water conditions. There were several relatively wet winters before 1945, and this was before the urbanization period following World War II and increased pumping of ground water.

Table 3 shows the yearly rainfall (in inches) at Hancock Park for the period between 1929 and 1973. For

Table 3
Rainfall in inches (Los Angeles-Hancock Park)

Year starting October	Annual total (in.)
1929/30	8.61
1930/31	12.47
1931/32	16.06
1932/33	13.65
1933/34	14.37
1934/35	21.27
1935/36	13.24
1936/37	21.85
1937/38	23.91
1938/39	17.20
1939/40	11.96
1940/41	34.78
1941/42	12.38
1942/43	18.13
1943/44	17.65
1944/45	13.29
1945/46	11.02
1946/47	14.19
1947/48	7.42
1948/49	8.63
1949/50	10.89
1950/51	8.51
1951/52	27.17
1952/53	10.99
1953/54	13.53
1954/55	10.84
1955/56	16.94
1956/57	12.21
1957/58	22.81
1958/59	7.40
1959/60	9.25
1960/61	5.69
1961/62	23.73
1962/63	10.66
1963/64	7.76
1964/65	14.65
1965/66	19.22
1966/67	23.78
1967/68	16.78
1968/69	24.85
1969/70	7.31
1970/71	13.37
1971/72	7.30
1972/73	20.50
Minimum	5.69
Maximum	34.78
Mean	14.96
Median	13.45

this period, the maximum rainfall was 34.78 in. (in 1940/41), and the minimum was 5.69 in. (in 1960/61). During the three years preceding the Long Beach earthquake, the rainfall was close to average (12.47, 16.06 and 13.65 in., respectively).

Fig. 9 shows the relative liquefaction susceptibility in the Los Angeles basin based on depths to ground water measured from 1960 to 1975. In comparison with Fig. 8, it can be seen that the development of the ground water resource can be effective in reducing or eliminating the liquefaction hazard. In this figure, the areas having very high (VH), high (H), or moderate (M) liquefaction susceptibility (if cohesionless, granular materials are present) occur only in restricted areas near the mouth of drainage, in harbor areas of Los Angeles, near Long Beach and Los Alamitos [45]. This shows that liquefaction susceptibility does vary with time and that in general it depends upon both natural and man-made factors, that lead to fluctuations in the depth to ground water.

Acknowledgements

I am indebted to Mr A. Walden of the Los Angeles County Department of Public Works, Water Resources Division, for providing the data for Table 3.

References

[1] Hauksson E, Gross S. Source parameters of the 1933 Long Beach earthquake. Bull Seism Soc Am 1991;81(1):81–98.
[2] Wood HO. Preliminary report on the Long Beach earthquake. Bull Seism Soc Am 1933;23(2):43–56.
[3] Neumann F. United States earthquakes (1933). US Department of Commerce Coast and Geodetic Survey, Serial No. 579; 1935. p. 9–14; also see p. 25–35.
[4] Campbell KW. A note on the distribution of earthquake damage in Long Beach, 1933. Bull Seism Soc Am 1976;66:1001–5.
[5] Martel RR. Earthquake damage to type III buildings in Long Beach, 1933. Earthquake investigations in the Western United States 1931–1964, US Coast and Geodetic Survey, Publ. 41-2; 1965. p. 213–22.
[6] Trifunac MD, Todorovska MI. Nonlinear soil response: 1994 Northridge, California, Earthquake. J Geotech Engng, ASCE 1996; 122(9):725–35.
[7] Trifunac MD, Todorovska MI. Nonlinear soil response as a natural passive isolation mechanism: 1994 Northridge, California earthquake. Soil Dynam Earthquake Engng 1998;17(1):41–51.
[8] Trifunac MD, Todorovska MI. Can aftershock studies predict site amplification factors? Northridge, California Earthquake of January 17, 1994. Soil Dynam Earthquake Engng 2000;19(4):233–51.
[9] Richter CF. Elementary seismology. San Francisco: Freeman and Co; 1958.
[10] Martel RR. A report on earthquake damage to type III buildings in Long Beach. Earthquake investigations in California 1934–1935, Special Publication, US Department of Commerce, Coast and Geodetic Survey; 1936. p. 143–62.
[11] Barrows AG. A review of the geology and earthquake history of the Newport-Inglewood structure zone. Special report 114, Los Angeles, CA: California Division of Mines and Geology; 1974.
[12] Eaton EJ. Long Beach, California, earthquake of March 10, 1933: geological notes. Bull Am Assoc Petrol Geol 1933;17(6):732–8.
[13] Yeates RS. Newport-Inglewood fault zone, Los Angeles Basin, California. Am Assoc Petrol Geol Bull 1973;57:117–35.
[14] Hillis D. Cracks produced by Long Beach, California, earthquake, geological notes. Bull Am Assoc Pet Geologists 1933;17(6):739–40.
[15] Trifunac MD, Brady AG, Hudson DE. Strong-motion earthquake accelerograms. II. Corrected accelerograms and integrated ground velocity and displacement curves. Report EERL 72-50. Earthquake Engineering Research Laboratory, California Institute of Technology, Pasadena, CA; 1973.

[16] Trifunac MD, Hudson DE, Brady AG. Strong-motion accelerograms. II. Corrected acceleration and integrated velocity and displacement curves. Report EERL 72-52. Earthquake Engineering Research Laboratory, California Institute of Technology, Pasadena, CA; 1975.
[17] Trifunac MD, Lee VW. Routine computer processing of strong-motion accelerograms. Report EERL 73-03. Earthquake Engineering Research Laboratory, California Institute of Technology, Pasadena, CA; 1973.
[18] Hudson DE. Golden anniversary workshop on strong-motion seismometry, March 30–31. Department of Civil Engineering Report, University of Southern California, Los Angeles, CA; 1983.
[19] Jordanovski LR, Todorovska MI. Inverse studies of the earthquake source mechanism from near-field strong motion records. Indian Soc Earthquake Tech J 2002;39(1/2):73–91.
[20] Benioff H. The determination of the extent of faulting with application to the Long Beach Earthquake. Bull Seism Soc Am 1938;28:77–84.
[21] Trifunac MD. Stress estimates for San Fernando, California earthquake of February 9, 1971: main event and thirteen aftershocks. Bull Seism Soc Am 1972;62:721–50.
[22] Trifunac MD. Broad band extension of Fourier amplitude spectra of strong-motion acceleration. Report No. CE 93-01. Department of Civil Engineering, University of Southern California, Los Angeles, CA; 1993.
[23] Ariman T, Muleski GE. A review of the response of buried pipelines under seismic excitations. Earthquake Engng Struct Dynam 1981; 9(2):133–51.
[24] Steinbrugge KV. Earthquakes, volcanoes and tsunamis: an anatomy of hazards. New York, NY: Skania America Group; 1982.
[25] Hoff NL. Earthquakes as a cause of major interruptions to gas service. Proceedings of Forty-first Annual Convention of the Pacific Coast Gas Association, Del Monte, California; 1934. p. 62–9.
[26] Bryant ES. The Long Beach Earthquake of March 10, 1933. Proceedings of Forty-first Annual Convention of the Pacific Coast Gas Association, Del Monte, California; 1934. p. 73–4.
[27] Zeng Y, Anderson JG. A composite source model of the 1994 Northridge earthquake using genetic algorithms. Bull Seism Soc Am 1996;86(1B):S71–S83.
[28] Trifunac MD. Tectonic stress and source mechanism of the imperial valley, California earthquake of 1940. Bull Seism Soc Am 1972;62: 1283–302.
[29] Todorovska MI, Trifunac MD. Distribution of pseudo spectral velocity during the Northridge, California, earthquake of 17 January, 1994. Soil Dynam Earthquake Engng 1997;16(3):173–92.
[30] Trifunac MD, Todorovska MI. Northridge, California, earthquake of January 17, 1994: density of red-tagged buildings versus peak horizontal velocity and site intensity of strong-motion. Soil Dynam Earthquake Engng 1997;16(3):209–22.
[31] Trifunac MD, Todorovska MI. Northridge, California earthquake of January 17, 1994: density of pipe breaks and surface strains. Soil Dynam Earthquake Engng 1997;16(3):193–207.
[32] Tinsley JC, Fumal TE. Mapping Quaternary Sedimentary Deposits for Areal Variations in Shaking Response. In: Ziony JI, editor. Evaluating Earthquake Hazards in the Los Angeles Region. Geological Survey Professional Paper 1360, Washington, DC; 1985. p. 101–25.
[33] Poland JF, Piper AM. Ground water geology of the coastal zone Long Beach-Santa Ana Area, California. US Geological Survey Water Supply Paper 1109, Washington, DC: US Government Printing Office; 1956.
[34] Thomas RG, Landry JJ, Turney RJ. Planned utilization of the groundwater basins of the coastal plain of Los Angeles county. California Department of Water Resources Bulletin No. 104. Appendix A: groundwater geology; 1961.
[35] Zielbauer EJ, Kves HA, Burnham WA, Keene AG. Coastal basin barrier and replenishment investigation-Dominguez gap barrier project geologic investigation. Los Angeles County Flood Control District, 29; 1962.
[36] Yerkes RF, McCulloh TH, Schoellhamer JE, Vedder JG. Geology of the Los Angeles Basin, California: an introduction. US Geological Survey Professional Paper 420-A; 1965.
[37] Milne J. Seismilogy, 2nd ed. London: Paul, Trench, Trubner, and Co; 1908.
[38] Kanai K. Relation between the nature of the surface layer and the amplitudes of earthquake motions. Bull Earthquake Res Inst, Univ Tokyo 1952;30(pt 1):31–7.
[39] Gutenberg B. Effects of ground on earthquake motion. Bull Seism Soc Am 1957;47:221–50.
[40] Medvedev JV. Engineering seismology. Israel program for scientific translations [available from US Department of Commerce, Clearing house for Federal Scientific and Technical Information, Springfield, VA.], Jerusalem; 1965.
[41] Lajoie KR, Helley EJ. Classification and mapping of quaternary sediments for purposes of seismic zonation. Studies for seismic zonation of the San Francisco Bay Region. US Geological Survey, Professional Paper 741-A, Washington, DC; 1975. p. A39–51.
[42] Tinsley JC, Youd TL, Perkins DM, Chen AT. Evaluating liquefaction potential. In: Ziony JI, editor. Evaluating earthquake hazards in the Los Angeles Region. US Geological Survey, Professional Paper 1360, Washington, DC; 1985. p. 263–315.
[43] Mendenhall WC. Development of underground waters in the Central Coastal Plain Region of Southern California. US Geological Survey Water-Supply Paper 138; 1905.
[44] Mendenhall WC. Development of underground waters in the Western Coastal Plain Region of Southern California. US Geological Survey Water-Supply Paper 139; 1905.
[45] Randell DH. Liquefaction potential in coastal areas in and around Long Beach, California. Unpublished MSc Thesis. California State University, Long Beach, CA; 1983.
[46] McFadden LD. The impact of temporal and spatial climatic changes on alluvial soils genesis in Southern California. Unpublished PhD Dissertation. University of Arizona 4308; 1982.
[47] Fumal TE, Tinsely JC. Mapping shear-wave velocities of near-surface geologic materials. In: Ziony JI, editor. Evaluating earthquake hazards in the Los Angeles region. US Geological Survey, Professional Paper 1360, Washington, DC; 1985. p. 127–49.